Journal of Environmental Chemical Engineering 12 (2024) 112097

Contents lists available at ScienceDirect

Journal of Environmental Chemical Engineering

journal homepage: www.elsevier.com/locate/jece

A novel CO_2 fixation catalyst FCO@NWs to synthesize benzimidazole at atmospheric pressure

Xuewei Tu [a], Yutong Chen [a], Can Sun [a], Yang Hu [a], Shouxin Zhu [a], Jingyi Qu [a], Zhexiao Zhu [a], Shijie Zhang [b,*], Hui Zheng [a,**]

[a] College of Material, Chemistry and Chemical Engineering, Hangzhou Normal University, Hangzhou 310000, PR China
[b] Hangzhou Synbest Biotech Co., Ltd., Hangzhou 310000, PR China

ARTICLE INFO

Editor: Jose Solla-Gullon

Keywords:
CO_2 fixation
Benzimidazole
Transition metal oxide
Nanowires

ABSTRACT

The utilization of CO_2 as an economical C1 feedstock for the production of valuable fine chemicals is widely recognized as a green and environmentally friendly approach. In this work, iron/cobalt oxide nanowires (FCO@NWs) composites were synthesized by a simple, convenient and cost-effective hydrothermal process. The FCO@NWs catalyst demonstrated efficient CO_2 fixation with *o*-phenylenediamine to produce benzimidazole at atmospheric pressure and 150 ℃. After 12 h reaction, the conversion rate of *o*-phenylenediamine reached an impressive 98%, indicating the catalyst's high efficiency in CO_2 fixation process. Through orthogonal experiments, the optimal reaction condition was confirmed and the application of the FCO@NWs catalyst for various *o*-phenylenediamine derivatives by substrate expansion was screened. Notably, this catalyst exhibited easy recoverability and reusability without significant loss in catalytic activity even after five cycles of experimentation. This study presents a promising approach for fixing CO_2 into valuable benzimidazole derivatives and contributes some experience to sustainable chemistry.

1. Introduction

Due to the rapid advancement of modern industry, the utilization of non-renewable energy sources such as fossil fuels have resulted in an escalating concentration of greenhouse gases like CO_2 in atmosphere [1,2]. This phenomenon has further exacerbated environmental issues including the greenhouse effect and glacier melting. Therefore, to mitigate these environmental challenges, there is a growing recognition that catalytic conversion of CO_2 directly into high value-added chemicals (such as methanol, formic acid, ethanol, cyclic carbonates and benzimidazole) represents a promising approach aligned with sustainable development [3–6]. Benzimidazole and its derivatives, as a value-added chemical, play an important role in drug synthesis [7,8]. For example, they serve as essential raw materials for synthesizing omeprazole, cimetidine, cyclobendazole, Marebavir, etc [9,10]. Benzimidazole and its derivatives are generally synthesized by the reaction of *o*-phenylenediamine with carboxylic acids, aldehydes, esters and aldehydes [11,12]. While the carbon sources used in these methods are often toxic and harmful [13]. From a green chemistry point of view, there is a strong desire to adopt a synthesis using inexpensive and non-toxic substrates like CO_2[14,15]. Nevertheless, due to the thermodynamic stability and kinetic inertia of CO_2, its conversion typically necessitates precious metal catalysts and harsh reaction conditions [16,17], thereby severely limiting its widespread industrial application. Consequently, it holds immense significance to develop simple, sustainable, and noble metal-free catalysts for the fixation of CO_2 to synthesize valuable chemicals.

In recent years, there has been a growing trend in the utilization of transition metals for CO_2 catalyzed reactions [18–20]. Due to their possession of d-orbital electrons or empty d-orbitals, these metals typically function as nucleophiles or electrophiles in chemical reactions [18], thereby facilitating the formation of intermediate products and lowering the activation energy required for the reaction. Iron, as an economically viable, environmentally friendly, easily recyclable, and abundantly available transition metal element, has garnered significant attention within the field of carbon sequestration research. However, the utilization of a single iron oxide catalyst is hindered by its low catalytic efficiency. Consequently, to enhance the effectiveness of the catalyst,

* Co-corresponding author.
** Corresponding author.
E-mail addresses: zhsj123@aliyun.com (S. Zhang), huizheng@hznu.edu.cn (H. Zheng).

https://doi.org/10.1016/j.jece.2024.112097
Received 5 November 2023; Received in revised form 29 December 2023; Accepted 29 January 2024
Available online 3 February 2024

various strategies can be employed such as doping with other metal ions, incorporating organic ligands, and optimizing the preparation process. These approaches aim to modify the crystal structure, surface morphology, and chemical composition of the catalyst in order to elevate its catalytic performance [21]. For instance, Li et al. enhanced the synthesis conditions through a hydrothermal method to prepare $FeVO_4$ nanowire catalysts. This approach effectively increased the active site density and conductivity of the catalyst, facilitating efficient transmission and migration of photogenerated carriers. Consequently, it significantly improved the catalytic efficiency for CO_2 conversion [22]. Duan et al. presented a heterojunction photocatalyst of Z-scheme Fe_2O_3/g-C_3N_4 for the reduction of CO_2 to methanol [23]. Yang et al. devised a single molecular structure multi-coordination Cu-Fe bimetallic MOF material (Cu-MOF-Fcdc-20%) that enhanced the selectivity of photocatalytic CO_2 reduction toward CO production [24]. Kosugi et al. employed iron porphyrin complexes to fabricate a catalyst with a supramolecular framework, which exhibited remarkable activity (29100 μmol g^{-1} h^{-1} for CO production, selectivity 99.9%) in reducing CO_2 under visible light irradiation [25]. As mentioned above, extensive research has been conducted on the utilization of iron-based catalysts for photocatalytic conversion of CO_2 to CO, CH_3OH and other C1 products. However, the application of iron-based catalysts in the conversion of CO_2 to benzimidazole derivatives remains limited. This is primarily due to the demanding conditions required for fixing CO_2 into benzimidazole derivatives, often necessitating high temperatures and pressures. For example, Matsuo et al. employed Al_2O_3 as a catalyst to facilitate the carbonylation reaction of o-phenylenediamine and CO_2 at 3.0 MPa and 170 ℃, resulting in the production of 2-benzimidazolones [26]. Liu and co-workers developed a $RuCl_2(dppe)_2$ catalyst for benzimidazole synthesis in the presence of CO_2 and H_2 atmosphere [27]. This method required excessively high pressures of CO_2 and H_2, along with the use of non-recyclable catalysts. Phatake et al. prepared a Cu@U-g-C_3N_4 catalyst using urea-derived porous graphite carbon nitrides (U-g-C_3N_4) and $CuCl_2$ as raw materials, successfully fixing CO_2 into benzimidazole at 2.5Mpa and 100 ℃ [28]. Hence, the development of novel iron-based catalysis with the ability to convert CO_2 into benzimidazole derivatives under milder conditions remains a challenge.

In this study, a series of composite catalysts consisting of Fe/Co oxide nanowires (FCO@NWs) were synthesized using a simple hydrothermal method. These catalysts demonstrated the ability to efficiently synthesize the pharmaceutical intermediate benzimidazole from *o*-phenylenediamine substrate and CO_2 under relatively mild conditions (1 atm) (Fig. 1). By conducting a comparative analysis of the catalysts employed in benzimidazole synthesis, it has been observed that our catalyst exhibits a yield comparable to that achieved under the corresponding reaction conditions (Table S1). The importance of bimetallic active sites was elucidated by comparing the catalytic activities of catalysts with varying ratios of Fe and Co. Furthermore, the catalyst exhibited a high robust nature, long-lived, and could be recycled up to five times under the experimental conditions. This work provides a new insight for designing catalysts aimed at converting CO_2 into benzimidazole derivatives.

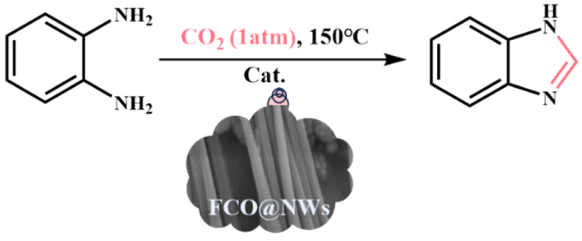

Fig. 1. General steps for the synthesis of benzimidazole with catalyst FCO@NWs.

2. Experimental

2.1. Materials

All chemicals and solvents were used without additional purification. CO_2 (99.99%) was supplied by Hangzhou Special Gases Factory. *o*-Phenylenediamine, Ammonium fluoride (NH_4F) and 4-Bromobenzene-1,2-diamine were provided by Aladdin Chemistry Co., Ltd. Cobalt (III) nitrate hexahydrate ($Co(NO_3)_2 \bullet 6\ H_2O$) and Ferric (III) nitrate hexahydrate ($Fe(NO_3)_3 \bullet 9\ H_2O$) were bought from Aladdin Reagent Co., Ltd. 4-Chlorobenzene-1,2-diamine, Deuterated solvent (DMSO-d_6), Dimethylamine borane (DMAB), and 1,2-Diamino-4-nitrobenzene were provided by Adamas Reagent Co., Ltd. 2-amino-4,5-dimethylphenylamine and N-hexane were provided by Energy Chemical. 2,3-diaminotoluene was provided by TCL (Shanghai) Development Co., Ltd. Urea was obtained by Yong Hua Chemical Co., Ltd. N,N-Dimethylformamide (DMF) and ethanol (EtOH) were purchased by Sinopharm Chemical Reagent Co., Ltd.

2.2. Synthesis of catalysts

A series of FCO@NWs were synthesized by one-step hydrothermal method. Typically, $Fe(NO_3)_3 \bullet 9\ H_2O$ (21.5, 16.6 and 12.5 mmol), $Co(NO_3)_2 \bullet 6\ H_2O$ (3.5, 8.3 and 12.5 mmol), CO $(NH_2)_2$ (25 mmol), NH_4F (5 mmol) and 25 mL deionized water (DIW) were added to 100 mL Teflon liner and mixed well for 30 min. This homogeneous was then kept at 150 ℃ for 7 h. The reaction conditions were determined based on previous literature [29] as well as initial experimental runs. The reaction product was air-cooled to room temperature and washed with EtOH and DIW several times. After filtration, dried at 80 °C for 6 h.

The prepared materials are denoted as F_6CO@NWs, F_2CO@NWs, and FCO@NWs, corresponding to Fe: Co molar ratios of 6: 1, 2: 1, and 1: 1 respectively. Similarly, CO@NWs was synthesized under the same conditions and without the addition of Fe.

2.3. General Procedure for the Synthesis of Benzimidazoles

The synthesis process of benzimidazole derivatives follows a similar procedure. *O*-phenylenediamine (1 mmol), catalyst (20 mg), DMAB (6.8 mmol), and DMF (5 mL) were taken in a 15 mL test tube. The mixture was then heated to 150 ℃ with continuous stirring, while CO_2 being bubbled into the solution, maintaining the CO_2 pressure at 1 atmosphere throughout the reaction. The progress of the reaction was monitored using thin layer chromatography (TLC, Methanol/Dichloromethane, V/V=1/10). After completion, the mixture was cooled to room temperature and the catalyst was separated through centrifugation. The extracted products were further purified by TLC and determined by ^1H NMR analysis (Fig. S1-S8).

Benzimidazole (2a)[14]. ^1H NMR (500 MHz, DMSO-d_6), δ8.20 (s, 1 H), 7.59 (m, 2 H), 7.19 (dd, J = 3.2, 6.1 Hz, 2 H).

5-Methylbenzimidazole (2b) [14]. ^1H NMR (500 MHz, DMSO-d_6), δ8.27 (s, 1 H), 7.72 (d, J = 7.8 Hz, 1 H), 7.66 (s, 1 H), 7.05 (d, J = 9.3 Hz, 1 H), 2.41 (s, 3 H).

4-Methyl-1 H-benzimidazole (2c) [30] . ^1H NMR (500 MHz, DMSO-d_6) δ 8.27 (s, 1 H), 7.34 (d, J = 8.55 Hz, 1 H), 7.08 (t, J = 7.54 Hz, 1 H), 6.96 (d, J = 7.31 Hz, 1 H), 1.95 (s, 3 H).

5, 6-Dimethylbenzimidazole (2d) [14] . ^1H NMR (500 MHz, DMSO-d_6) δ 8.29 (s, 1 H), 7.43 (s, 2 H), 2.30 (s, 6 H).

5-Chlorobenzimidazole (2e) [14]. ^1H NMR (500 MHz, DMSO-d_6) δ 8.31 (s, 1 H), 7.66 (d, J = 1.81 Hz, 1 H), 7.61 (d, J = 8.77 Hz, 1 H), 7.21 (dd, J = 1.88, 8.44 Hz, 1 H).

5-Flurobenzimidazole (2 f) [30]. ^1H NMR (500 MHz, DMSO-d_6) δ 8.28 (s, 1 H), 7.60 (dd, J = 9, 4,5, 1 H), 7.39 (dd, J = 8.9, 2.4 Hz, 1 H), 7.06 (td, J =9.5, 2 Hz, 1 H).

5-Bromobenzimidazole (2 g) [30]. ^1H NMR (500 MHz, CDMSO-d_6) δ 8.33 (s, 1 H), 7.86 (s, 1 H), 7.60 (d, J = 8.50 Hz, 1 H), 7.36 (d, J =

8.87 Hz, 1 H).

5-Nitrobenzimidazole (2 h) [27]. ^{1}H NMR (500 MHz, DMSO-d_6) δ 8.54 (s, 1 H), 8.46 (d, J = 3.3 Hz, 1 H), 8.32 (d, J = 3.2, Hz, 1 H), 7.85 (dd, J = 2.6, 9.5 Hz, 1 H).

3. Results and discussion

3.1. Phase and morphology analysis

The crystal structure of the synthesized FCO@NWs in varying proportions was characterized by X-ray powder diffraction (XRD). The results in Fig. 2 demonstrate that the major diffraction peaks of FCO@NWs, F_2CO@NWs and F_6CO@NWs can all be attributed as β-FeOOH of pure rhomboid structure, which is consistent with the standard card JCPDS no.775–1594. However, with the increase of Co content, peaks of $CoCO_3$ appear gradually in F_2CO@NWs and FCO@NWs, and diffraction peaks of about 25.0° and 32.6° correspond to the (0 1 2) and (1 0 4) planes of $CoCO_3$ (JCPDS no.78–0209), respectively. The results indicate that iron/cobalt oxide nanowires composites were successfully synthesized. Strong and sharp diffraction peaks indicate that FCO@NWs, F_2CO@NWs and F_6CO@NWs are highly crystalline. In fact, there is no characteristic diffraction peak of Co on the catalyst F_6CO@NWs. This may be due to the relatively low Co content and the fact that the radius of atomic Co is slightly smaller than the radius of Fe, so the structure of F_6CO@NWs is consistent with that of FeOOH.

The morphology of the CO@NWs, F_6CO@NWs, F_2CO@NWs and FCO@NWs catalysts was examined using scanning electron microscopy (SEM), while mapping analysis was employed to determine the elemental composition of the FCO@NWs surface. Fig. 3(a) reveals that the CO@NWs possess a large size with multiple nanowires arranged in a spherical agglomeration. While this structure may enhance the surface area, it hampers the transport of active substances, leading to diminished catalytic activity. Conversely, Fig. 3(b) demonstrates that F_6CO@NWs possess a smooth surface and a stacked structure, thereby enhancing both catalyst stability and the efficiency of active substance catalysis. Additionally, each nanowire's size is less than 100 nm, providing direct evidence for successful synthesis. As depicted in Fig. 3 (c), compared with F_6CO@NWs, there are more defects and more active sites at the end of FCO@NWs, thus increasing the catalytic activity. Consequently, this enhances both the quantity of active sites and catalytic efficiency. Furthermore, apart from the nanowires, observable fragments are evident in FCO@NWs, which can be attributed to the elevated Co content. Additionally, some free $CoCO_3$ nanoparticles are observed, which is also consistent with the conclusion of XRD. Subsequently, by analyzing the elements of FCO@NWs (Fig. 3(d)), the results showed that the catalyst was homogeneously dispersed with Fe and Co elements, indicating the successful synthesis of the FCO@NWs catalyst. For an in-depth detection of the structure and morphology of FCO@NWs, the transmission electron microscopy (TEM) images are shown in Fig. 3(e)-(f). According to the arc edge depicted in Fig. (e), the presence of a stacked structure comprising multiple nanowires can be observed, which is consistent with the SEM images. Notably, Fig. 3(f) reveals distinct lattice fringe spacing. Specifically, β-FeOOH (1 3 0) exhibited a lattice spacing of 0.331 nm, and the $CoCO_3$ (1 0 4) displayed a lattice spacing of 0.274 nm. These values are consistent with the XRD pattern, providing compelling evidence for the successful synthesis of the catalyst. The Brunauer-Emmett-Teller (BET) N_2 adsorption-desorption isotherm and Barrett-Joyner-Halenda (BJH) were used to obtain the specific surface area and pore size distribution of FCO@NWs samples (Fig. 3(g)). The BET curve depicted in Fig. 3(g) exhibits the type III curve of the H3 hysteresis loop. The samples possess a specific surface area and pore size of 6.70 m^2/g^{-1} and 11.1 nm, respectively. The pore size distribution diagram reveals that the predominant porosity is mesoporous and macroporous, with fewer pores present, resulting in reduced N_2 adsorption and consequently a smaller measured specific surface area. This observation aligns with the SEM results obtained as well.

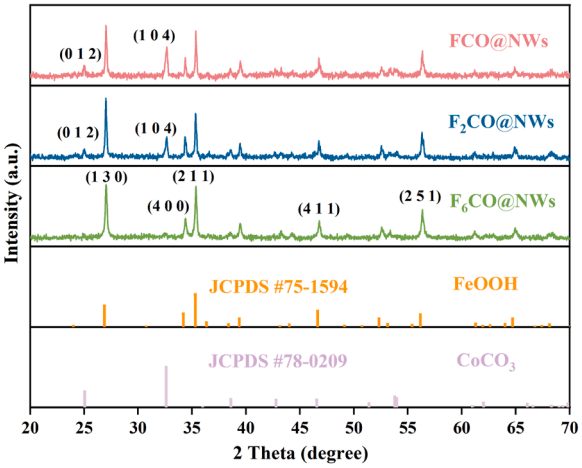

Fig. 2. XRD patterns of CO@NWs, FCO@NWs, F_2CO@NWs and F_6CO@NWs.

3.2. Chemical composition and states

The chemical composition and oxidation state of the catalyst were confirmed through X-ray photoelectron spectroscopy (XPS) (Fig. 4). The XPS spectra of all elements were adjusted for C 1 s (binding energy at 284.80 eV). As depicted in Fig. 4(a), the FCO@NWs catalyst comprises four elements (C, O, Fe, and Co), which aligns with the components of F_6CO@NWs. In Fig. 4(b), Fe $2p_{1/2}$ peaks (binding energy at 726.8 eV and 724.4 eV) along with Fe $2p_{2/3}$ peaks (binding energy at 711.2 eV and 713.8 eV) indicate that the catalyst exists in both Fe^{2+} and Fe^{3+} forms [29]. Also, Fig. 4(c) shows the refined spectra of Co 2p with the primary peaks of Co $2p_{3/2}$ and Co $2p_{1/2}$ positioned at 779.2 eV and 794.4 eV [29], respectively. The results demonstrate that Fe and Co oxides are not exist independently in the catalyst, but interact with each other, which also proves the successful preparation of F_6CO@NWs composites. Furthermore, Fig. 4(d) displays the deconvolution analysis of the O1s XPS peak revealing two distinct component peaks at 529.5 eV and 531.3 eV, corresponding to the Co-O and Fe-O peaks respectively, which is also consistent with the previous characterization results.

3.3. Active sites and basicity

To understand the nature of the interaction of CO_2 with the catalyst at high temperature, temperature-programmed desorption of carbon dioxide (CO_2-TPD) were performed. CO_2-TPD was conducted with helium (30–50 mL/min) as the carrier gas, at a heating rate of 10 °C/min over a temperature range of 50–500 °C. Fig. 5 displays the CO_2-TPD profiles of the catalyst, revealing three distinct desorption peaks for FCO@NWs catalyst. An intermediate temperature peak at 251 ℃ indicates medium strength basic sites on the surface related to acid-base Lewis pairs [31], while high temperature peaks (400–500 ℃) correspond to strong basic sites associated with low coordination surface O^{2-} [32]. In addition, there is basically no CO_2 desorption in the catalyst within 200 ℃, indicating that the adsorption of CO_2 at the active site of the catalyst is relatively stable at this temperature. This is also consistent with the results of the optimization of experimental conditions.

3.4. Exploration and optimization of experimental conditions

To obtain the optimal experimental condition, the reaction temperature, reaction time and catalyst amount were optimized by orthogonal experiment with *o*-phenylenediamine as substrate and the amount of reducing agent (DMAB) unchanged. The specific experimental condition

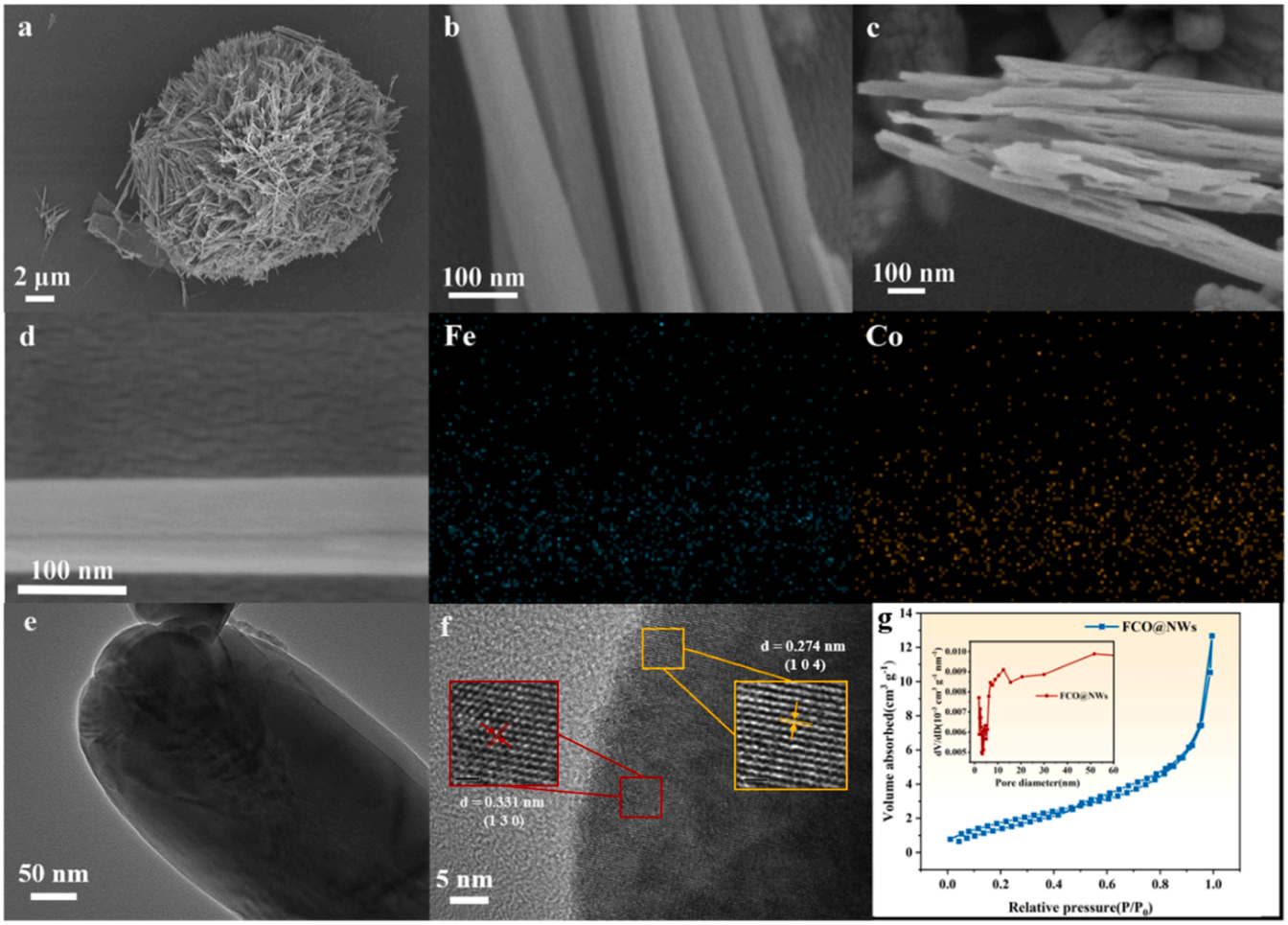

Fig. 3. SEM image of (a) CO@NWs, (b) F_6CO@NWs, (c) FCO@NWs, (d) mapping of FCO@NWs, (e) TEM image of FCO@NWs, (f) HRTEM of FCO@NWs and (g) Nitrogen adsorption desorption isotherms of FCO@NWs and the corresponding pore size distribution.

design and results analysis are shown in Tables 1–3.

Table 1 shows three factors and three levels: reaction temperature (90 ℃, 120 ℃ and 150 ℃), reaction time (6 h, 9 h, 12 h) and catalyst amount (10 mg, 20 mg, 30 mg). The substrate conversion rate under various conditions is presented in Table 2. The optimal reaction condition is determined by the K value (where K1 represents the average yield of Entry1, 2 and 3 in Table 2) associated with each factor. A higher K value indicates a superior level for that specific factor, implying that greater yields can be achieved under the corresponding experimental conditions. The maximum K values of reaction temperature, reaction time and catalyst dosage in Table 3 are K3 (84), K3 (86) and K3 (77), respectively. Consequently, based on the analysis of the orthogonal experiment results, it is evident that the optimal experimental conditions entail a reaction temperature of 150 ℃, a reaction time of 12 h, and a catalyst amount of 30 mg. Furthermore, considering that the R value signifies the extent to which various factors influence the reaction outcomes, it can be concluded that the reaction time corresponding to the highest R value (23) exerts the most significant influence on catalyst yield, while catalyst amount exhibits minimal impact.

3.5. Comparison of catalyst performance

Under optimized experimental conditions (150 ℃, 12 h and 30 mg catalyst), CO_2 fixation experiments were conducted to explore the effects of different iron and cobalt ratios on the catalytic efficiency (Fig. 5). The findings indicate a noticeable enhancement in catalytic efficiency with increasing Co content. However, the performance of simple CO@NWs catalyst is unsatisfactory. This can be attributed to the synergistic effect between iron oxides and cobalt oxides, which amplifies the active sites within the nanowires and consequently significantly improves catalytic efficiency.

3.6. Substrate screening

The application range and limitations of the FCO@NWs catalyst were investigated through the utilization of various *o*-phenylenediamine derivatives in catalytic reactions, conducted under optimal experimental conditions (refer to Table 4).

The results demonstrate the exceptional yields of various *o*-phenylenediamine derivatives with diverse electron donating/withdrawing groups. Notably, substrates possessing electron donor groups (Table 4, entries 1, 2 and 3) exhibit high efficiency in producing the corresponding benzimidazole derivatives. Conversely, when utilizing substrates with electron withdrawing groups (Table 4, entries 4, 5 and 6), a slightly reduced yield is observed. This phenomenon can be attributed to the increased electron density on the benzene ring due to interaction with the electron donating group, thereby promoting cyclization reactions. However, when 1,2-Diamino-4-nitrobenzene was used as the substrate, the catalytic yield also decreased slightly. This phenomenon can be attributed to the pronounced electron-absorbing effect exhibited by nitrobenzene, which consequently diminishes the electron density within the benzene ring and impedes efficient cyclization. In an effort to expand substrate scope further, *o*-aminothiophenol was also investigated. However, no significant transformation was detected, possibly

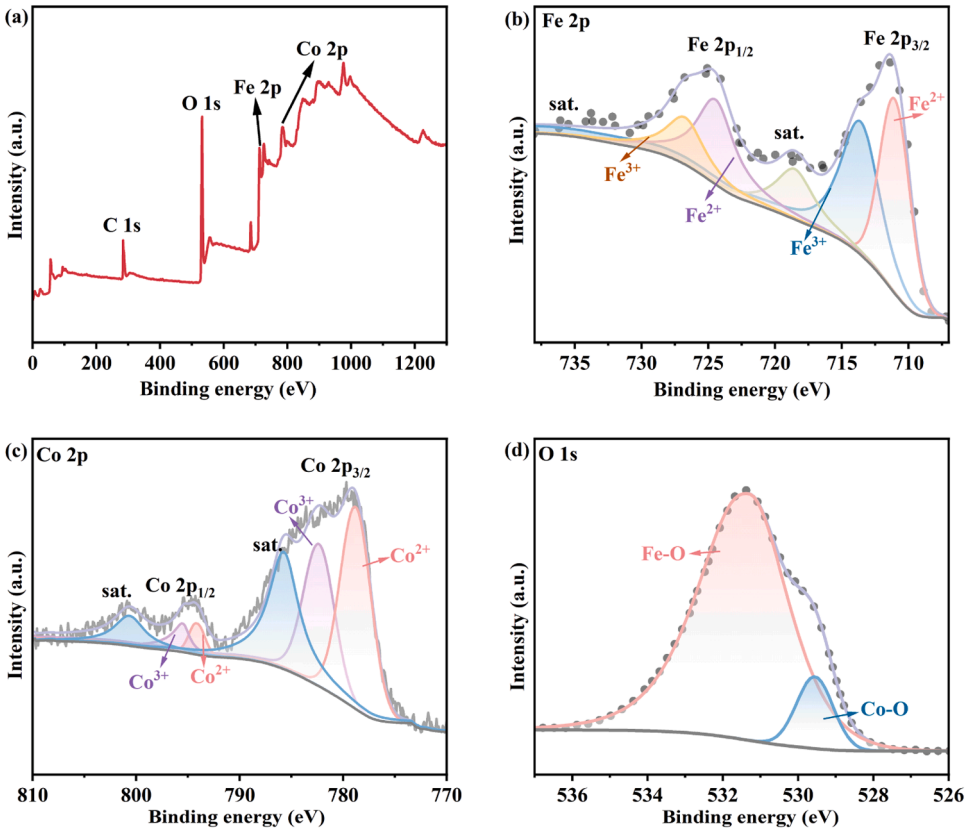

Fig. 4. (a) The XPS spectra of F_6CO@NWs (b) Fe 3d, (c) Co 2p, (d) O 1 s.

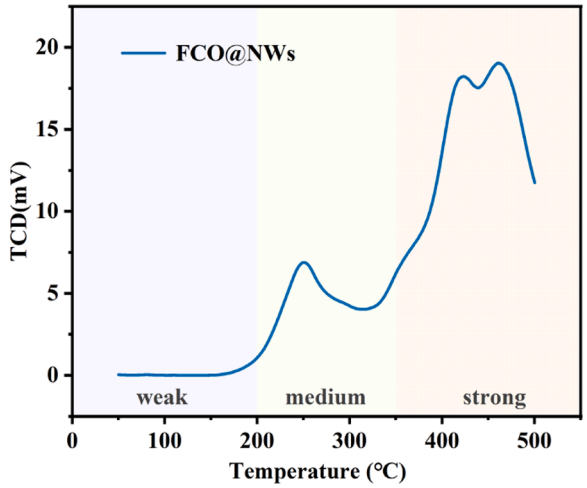

Fig. 5. CO_2-TPD of the FCO@NWs.

Table 1
Orthogonal experimental design.

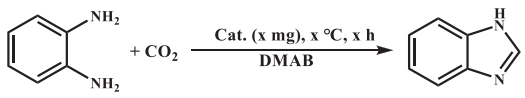

Entry	Temperature (℃)	Time (h)	Cat. (mg)
1	90	6	10
2	120	9	20
3	150	12	30

Table 2
Orthogonal experimental results.

Entry	Temperature (℃)	Time (h)	Cat. (mg)	Yield (%)[a]
1	90	6	10	50
2	90	9	20	67
3	90	12	30	75
4	120	6	20	60
5	120	9	30	78
6	120	12	10	90
7	150	6	30	78
8	150	9	10	83
9	150	12	20	92

Reaction condition: catalyst (x mg), x ℃, x h, *o*-phenylenediamine (1 mmol), DMAB (6.8 mmol), and DMF (5 mL), (x represents the corresponding value in the orthogonal experiment (Table 2))

[a] Yield based on GC analysis.

Table 3
Analysis of the results.

Entry	Temperature (℃)	Time (h)	Cat. (mg)
K1	64	62	74
K2	76	76	73
K3	84	86	77
R	20	23	4

due to limited reactivity between the substrate and CO_2.

3.7. *Recyclability study*

To investigate the recyclability and stability of the FCO@NWs catalyst, we employed *o*-phenylenediamine as a substrate to catalyze CO_2 fixation for benzimidazole synthesis under optimized experimental

Table 4
Synthesis of various benzimidazoles.

Entry	Substrate	Product	Yield (%)[a]
1	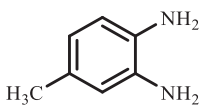	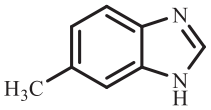	93
2	1a 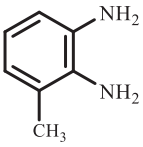	2a 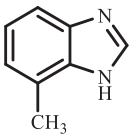	90
3	1b 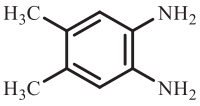	2b 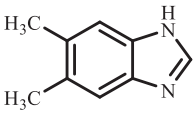	96
4	1c 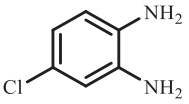	2c 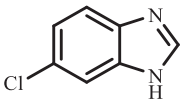	80
5	1d 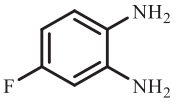	2d 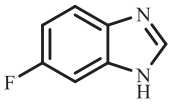	88
6	1e 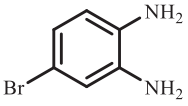	2e 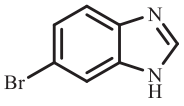	84
7	1 f 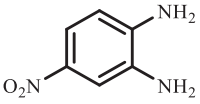	2 f 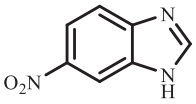	81
8	1 g 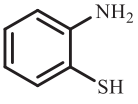 1 h	2 g 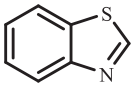 2 h	trace

Reaction condition: substrate (1 mmol), catalyst (30 mg), DMAB (6.8 mmol), and DMF (5 mL), 150 ℃, 12 h.
[a] GC yield.

conditions (Fig. 6). After each cycle, the catalyst was easily separated through simple centrifugation and subsequently washed three times with DMF and EtOH separately. Subsequently, the washed catalyst was subjected to vacuum drying at 80 ℃ for 7 h in preparation for the subsequent cycle experiment. Remarkably, our results demonstrate that even after undergoing five cycles, the synthesized FCO@NWs catalyst remains sufficiently stable, highlighting its potential as a highly stable and readily recoverable catalyst option. To confirm the structural stability of the catalyst, a comparison was made between the structure of the freshly prepared catalyst and that after a single catalysis (Fig. S9). The results indicate that following experimentation, there were no significant changes to the structure of the catalyst, with only a slight decrease in crystallinity observed. These findings provide evidence for excellent structural stability exhibited by this particular catalyst. Fig. 7.

3.8. Exploration of mechanism

Based on the previous literature, a tentative reaction mechanism for the synthesis of benzimidazole was proposed (Fig. 8) [33,34]. Initially, the catalyst FCO@NWs activates DMAB to generate intermediate II. Subsequently, FCO@NWs catalyzes the CO_2 insertion into the B-H bond, leading to the formation of intermediate III. Intermediate III then undergoes a reaction with one of the amino groups present in o-phenylenediamine resulting in formamide intermediate IV (during this process, DMAB serves as an environmentally friendly and safe reducing agent). Finally, formamide cyclization undergoes dehydration to produce the desired product benzimidazole.

4. Conclusion

In summary, benzimidazole derivatives were successfully synthesized by fixing CO_2 under atmospheric pressure at 150 ℃ using FCO@NWs catalyst. Controlled experiments demonstrated that the addition of Co oxide enhanced the active sites of the catalyst, facilitated the formation of the desired product, and significantly improved the catalytic efficiency of the iron-based catalyst. This strategy enables both CO_2 reduction and construction of two C-N bonds for nitrogen-containing heterocyclic compound synthesis. The cost-effective, stable, and efficient nature of this catalytic system holds promising potential for utilizing CO_2 as a high value-added product under mild conditions.

CRediT authorship contribution statement

Zheng Hui: Funding acquisition, Project administration, Supervision, Writing – review & editing. **Zhang Shijie:** Funding acquisition. **Tu Xuewei:** Data curation, Formal analysis, Investigation, Methodology,

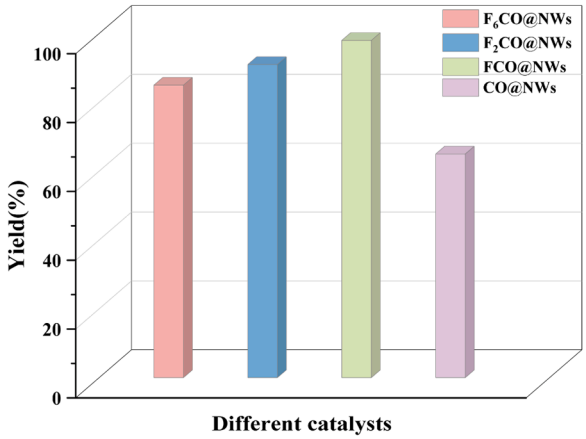

Fig. 6. Comparison of catalytic performance of different catalysts under optimal conditions.

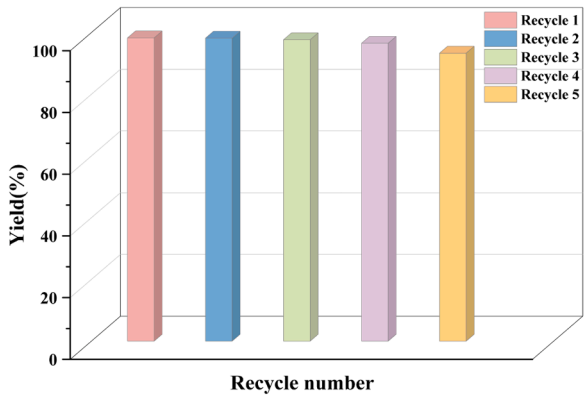

Fig. 7. Cycle test of FCO@NWs catalyst for the synthesis of benzimidazole under optimal conditions.

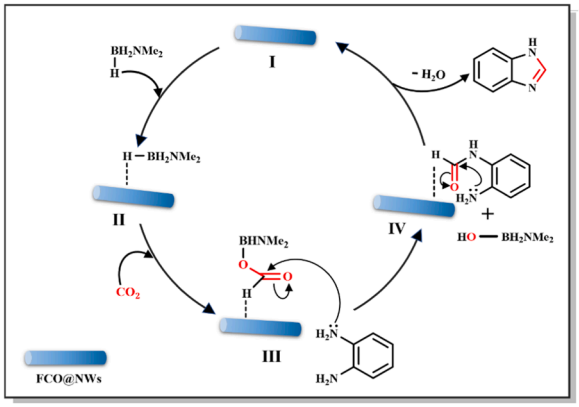

Fig. 8. The plausible mechanism for the synthesis of benzimidazole from *o*-phenylenediamine and DMAB via catalyst fixation of CO_2.

Project administration, Writing – original draft. **Sun Can:** Investigation, Resources, Supervision. **Zhu Shouxin:** Methodology, Validation. **Hu Yang:** Data curation, Investigation. **Chen Yutong:** Formal analysis, Methodology, Project administration, Writing – review & editing. **Qu Jingyi:** Investigation. **Zhu Zhexiao:** Investigation.

Declaration of Competing Interest

All authors declare that they have no conflict of interest.

Data availability

The data that has been used is confidential.

Acknowledgements

This work was supported by the National Natural Science Foundation of China (Grant NO. 21978061).

Appendix A. Supporting information

Supplementary data associated with this article can be found in the online version at doi:10.1016/j.jece.2024.112097.

References

[1] Y. Zhang, L. Cao, G. Bai, X. Lan, Engineering single Cu sites into covalent organic framework for selective photocatalytic CO_2 Reduction, Small 19 (2023) e2300035.
[2] Z. Zeng, Y. Yan, J. Chen, P. Zan, Q. Tian, P. Chen, Boosting the photocatalytic ability of Cu_2O nanowires for CO_2 conversion by MXene quantum dots, Adv. Funct. Mater. 29 (2018).
[3] R. Verma, R. Belgamwar, V. Polshettiwar, Plasmonic photocatalysis for CO_2 conversion to chemicals and fuels, ACS Mater. Lett. 3 (2021) 574–598.
[4] Z. Wu, W. Li, L. Hou, Q. Wei, H. Yang, Y. Jiang, D. Tang, A novel Sunflower-like MOF@COF for improved photocatalytic CO_2 reduction, Sep. Purif. Technol. 311 (2023).
[5] J.T. Ren, Y.L. Zheng, K. Yuan, L. Zhou, K. Wu, Y.W. Zhang, Self-templated synthesis of Co_3O_4 hierarchical nanosheets from a metal-organic framework for efficient visible-light photocatalytic CO_2 reduction, Nanoscale 12 (2020) 755–762.
[6] B.M. Pirzada, A.H. Dar, M.N. Shaikh, A. Qurashi, Reticular-chemistry-inspired supramolecule design as a tool to achieve efficient photocatalysts for CO_2 reduction, ACS Omega 6 (2021) 29291–29324.
[7] Z. Ye, J. Chen, Sulfonate-grafted metal-organic frameworks for reductive functionalization of CO_2 to benzimidazoles and N-formamides, ACS Catal. 11 (2021) 13983–13999.
[8] Z. Zhang, Q. Sun, C. Xia, W. Sun, CO_2 as a C1 Source: $B(C_6F_5)_3$-catalyzed cyclization of o-phenylene-diamines to construct benzimidazoles in the presence of hydrosilane, Org. Lett. 18 (2016) 6316–6319.
[9] R. Khatun, S. Biswas, I.H. Biswas, S. Riyajuddin, N. Haque, K. Ghosh, S.M. Islam, Cu-NPs@COF: a potential heterogeneous catalyst for CO_2 fixation to produce 2-oxazolidinones as well as benzimidazoles under moderate reaction conditions, J. CO_2 Util. 40 (2020).
[10] V. Francesconi, E. Cichero, S. Schenone, L. Naesens, M. Tonelli, Synthesis and biological evaluation of novel (thio)semicarbazone-based benzimidazoles as antiviral agents against human respiratory viruses, Molecules 25 (2020).
[11] R.-X. Gao, Y.-Y. Gao, N. Zhu, L.-M. Han, CO_2 improved synthesis of benzimidazole with the catalysis of a new calcium 4-amino-3-hydroxybenzoate, Acta Chim. Slov. 68 (2021) 205–211.
[12] D. Raja, A. Philips, P. Palani, W.Y. Lin, S. Devikala, G.C. Senadi, Metal-free synthesis of benzimidazoles via oxidative cyclization of d-glucose with o-phenylenediamines in water, J. Org. Chem. 85 (2020) 11531–11540.
[13] M. Brahmayya, S.A. Dai, S.-Y. Suen, Facile synthesis of 2-benzimidazolones via carbonylation of o-phenylenediamines with CO_2, J. CO_2 Util. 22 (2017) 135–142.
[14] L. Hao, Y. Zhao, B. Yu, H. Zhang, H. Xu, Z. Liu, Au catalyzed synthesis of benzimidazoles from 2-nitroanilines and CO_2/H_2, Green. Chem. 16 (2014).
[15] M. Hulla, S. Nussbaum, A.R. Bonnin, P.J. Dyson, The dilemma between acid and base catalysis in the synthesis of benzimidazole from o-phenylenediamine and carbon dioxide, Chem. Commun. (Camb.) 55 (2019) 13089–13092.
[16] X. Cao, H.A. Zhong, P. Zhang, H. Zheng, The simple system of fixing CO_2 to synthesize benzimidazolones at atmospheric pressure, J. CO_2 Util. 24 (2018) 250–255.
[17] L. Zhang, X. Tu, Y. Chen, W. Han, L. Chen, C. Sun, S. Zhu, Y. Song, H. Zheng, Photothermal catalysis without solvent for fixing CO_2 to cyclic carbonate, Mol. Catal. 538 (2023).
[18] L. Shi, P. Wang, Q. Wang, X. Ren, F. Ichihara, W. Zhou, H. Zhang, Y. Izumi, B. Cao, S. Wang, H. Chen, J. Ye, Efficient photocatalytic CO_2 reduction mediated by transitional metal borides: metal site-dependent activity and selectivity, J. Mater. Chem. A 8 (2020) 21833–21841.
[19] L. Zhang, X. Tu, Y. Chen, S. Zhu, C. Sun, Y. Song, H. Zheng, Synthesis of cyclic carbonates by photothermal catalytic coupling of CO_2 and epoxides under solvent-free conditions, Appl. Catal. A: Gen. 666 (2023).
[20] S. Shaheen, S.A. Ali, U.F. Mir, I. Sadiq, T. Ahmad, Recent advances in transition metal phosphide nanocatalysts for H_2 evolution and CO_2 reduction, Catalysts 13 (2023).
[21] F. Wu, L. Wan, Q. Li, Q. Zhang, B. Zhang, Ternary assembled MOF-derived composite: anisotropic epitaxial growth and microwave absorption, Compos. Part B: Eng. 236 (2022).
[22] Y. Li, Z. Zeng, Y. Chen, Y. Zhang, W. Wang, X. Xu, M. Du, Z. Li, Z. Zou, FeVO4 nanowires for efficient photocatalytic CO_2 reduction, Catal. Sci. Technol. 12 (2022) 3289–3294.
[23] B. Duan, L. Mei, A. Z-scheme, Fe_2O_3/g-C_3N_4 heterojunction for carbon dioxide to hydrocarbon fuel under visible illuminance, J. Colloid Interface Sci. 575 (2020) 265–273.
[24] H. Yang, M. Zhang, Z. Guan, J. Yang, Cu-Fe bimetallic MOF enhances the selectivity of photocatalytic CO_2 reduction toward CO production, Catal. Sci. Technol. (2023).
[25] K. Kosugi, C. Akatsuka, H. Iwami, M. Kondo, S. Masaoka, Iron-complex-based supramolecular framework catalyst for visible-light-driven CO_2 reduction, J. Am. Chem. Soc. 145 (2023) 10451–10457.
[26] H. Matsuo, J.-C. Choi, T. Fujitani, K.-i Fujita, Carbonylation of o-phenylenediamines with CO_2 to 2-benzimidazolones catalyzed by alumina, Tetrahedron Lett. 96 (2022).
[27] Q. Liu, L. Wu, R. Jackstell, M. Beller, Using carbon dioxide as a building block in organic synthesis, Nat. Commun. 6 (2015) 5933.
[28] V.V. Phatake, B.M. Bhanage, Cu@U-g-C_3N4 catalyzed cyclization of o-phenylenediamines for the synthesis of benzimidazoles by using CO_2 and dimethylamine borane as a hydrogen source, Catal. Lett. 149 (2018) 347–359.
[29] M. Usman, M.T. Ahsan, S. Javed, Z. Ali, Y. Zhan, I. Ahmed, S. Butt, M. Islam, A. Mahmood, M.A. Akram, Facile synthesis of iron nickel cobalt ternary oxide (FNCO) mesoporous nanowires as electrode material for supercapacitor application, J. Mater. 8 (2022) 221–228.
[30] X. Li, J. Zhang, Y. Yang, H. Hong, L. Han, N. Zhu, Reductive cyclization of o-phenylenediamine with CO_2 and BH_3NH_3 to synthesize 1H-benzoimidazole derivatives, J. Organomet. Chem. 954-955 (2021).

[31] D. Wierzbicki, R. Baran, R. Dębek, M. Motak, M.E. Gálvez, T. Grzybek, P. Da Costa, P. Glatzel, Examination of the influence of La promotion on Ni state in hydrotalcite-derived catalysts under CO_2 methanation reaction conditions: Operando X-ray absorption and emission spectroscopy investigation, Appl. Catal. B: Environ. 232 (2018) 409–419.

[32] F. Han, H. Liu, W. Cheng, Q. Xu, Highly selective conversion of CO_2 to methanol on the CuZnO-ZrO_2 solid solution with the assistance of plasma, RSC Adv. 10 (2020) 33620–33627.

[33] A. Helal, M.A. Sanhoob, B. Hoque, M. Usman, M.H. Zahir, Bimetallic metal-organic framework derived nanocatalyst for CO_2 fixation through benzimidazole formation and methanation of CO_2, Catalysts 13 (2023) 12.

[34] I.H. Biswas, S. Biswas, M.S. Islam, S. Riyajuddin, P. Sarkar, K. Ghosh, S.M. Islam, Catalytic synthesis of benzimidazoles and organic carbamates using a polymer supported zinc catalyst through CO_2 fixation, N. J. Chem. 43 (2019) 14643–14652.